18:1 Pressure Ratio Axial/Centrifugal Compressor Demonstration Program

Jeffrey K. Schweitzer*
Pratt & Whitney Aircraft, West Palm Beach, Florida
and
John W. Fairbanks†
U.S. Department of Energy, Washington, D.C.

The results of a component technology demonstration program to design and test an advanced axial/centrifugal compressor for industrial gas turbine applications are presented. Objectives were to demonstrate 18:1 pressure ratio at 90% polytropic efficiency with 80% fewer parts as compared to current industrial gas turbine compressors. The compressor design approach utilizes low-aspect-ratio/highly loaded axial compressor blading combined with a centrifugal backend stage to achieve the 18:1 design pressure ratio on a single spool in only seven stages. Demonstrated design point performance was 91.5% polytropic efficiency at 14% stall margin and 70 lbm/s flow. This represents the highest known demonstrated performance in this pressure ratio and flow class. The results are particularly significant in that they were accomplished at axial compressor aerodynamic loading levels approximately 15% above current production engine design practice.

Nomenclature

D_f = diffusion factor
h = enthalpy, Btu/lbm
N = rotor speed, rpm
P = static pressure, psia
P_T = total pressure, psia
PR = pressure ratio
T = total temperature, °R
w = relative velocity, ft/s
W = flow rate, lbm/s
γ = ratio of specific heats
δ = $P_{T1}/14.696$
η = efficiency
θ = $T_1/518.688$

Subscripts

1 = inlet plenum instrumentation station
2 = axial compressor discharge instrumentation station
3 = pipe diffuser exit plane instrumentation station
ad = adiabatic
bl = interstage bleed flow
cor = corrected to standard day inlet conditions
net = corrected for interstage bleed
p = polytropic

Introduction

A CONCERTED national effort is currently in progress to conserve energy and increase utilization of our abundant domestic energy resources. As a part of this effort the U.S. Department of Energy's (DOE) Office of Coal Utilization has assigned high priority to supporting the development of advanced industrial/utility gas turbine engines for operation in combined cycle systems on coal-derived fuels. The strategy for large central power systems is to assist the development of high-temperature (2600-3000°F), high-performance, nominal 100 MW size gas turbines combined with efficient waste heat boilers and steam turbines. The primary fuel for the central power system is coal gasification. Dispersed power system support for the 5-50 MW range gas turbine, either simple or combined cycle, includes the development of advanced gas turbine component technology and multifuel capability.

In January 1976, a contract was awarded to Pratt & Whitney Aircraft Government Products Division (P&WA/GPD) to investigate the utilization of advanced aircraft gas turbine technology to improve the performance and durability of future industrial gas turbines in either the central or dispersed power system applications. Additional emphasis was placed on significantly reducing the number of gas turbine parts to improve reliability, lower initial cost, and thus enhance commercialization whether through retrofit of existing systems or through incorporation in a new centerline engine.

In phase I of the program,[1] the latest aircraft gas turbine technology was applied in the definition of a conceptual advanced gas turbine in the 15,000 shp/10 MW class (Fig. 1). The design approach included designing to higher cycle pressure ratio (18:1) and combustor exit temperature (2500°F) for increased cycle efficiency and specific power. Predicted simple-cycle performance potential of the conceptual engine was 13,856 shp at 36.3% thermal efficiency. Performance potential in combined cycle operation approaches 50% thermal efficiency depending on the type of waste heat recovery system utilized.

The compressor design for this conceptual engine incorporated highly loaded low-aspect-ratio axial compressor blading combined with a centrifugal back end stage to attain a polytropic efficiency goal of 90% with minimum number of stages. The reduced number of stages in combination with the inherent stiffness of the single-piece axial compressor drum rotor configuration additionally enabled consideration of a single-shaft gas generator without requiring a third bearing compartment in the hot section area. It is of interest to note that while the compressor design techniques employed are at the forefront of current compressor technology, the concept of axial stages followed by a centrifugal stage was included in Sir Frank Whittle's original aircraft gas turbine engine patent disclosure in 1930.

The present paper describes the results of the compressor component demonstration testing conducted under phase II

Presented as Paper 81-1479 at the AIAA/SAE/ASME 17th Joint Propulsion Conference, Colorado Springs, Colo., July 27-29, 1981; submitted Aug. 12, 1981; revision received Sept. 20, 1982.

*Design Technology Specialist, Goverment Products Division. Member AIAA.

†Program Manager, Heat Engines Branch, Office of Coal Utilization.

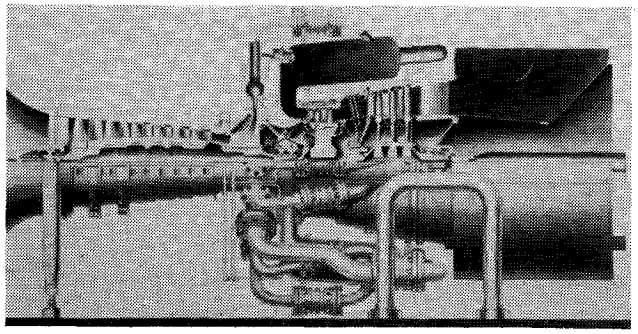

Fig. 1 Advanced technology 10 MW industrial gas turbine.

of the above program. A full-scale compressor test rig was designed, fabricated, and tested in the P&WA/GPD compressor test facility located in West Palm Beach, Fla. Performance characteristics of both the axial and centrifugal compressor stages as well as that of the overall compressor were documented over the entire compressor operating range. The results of this compressor development have subsequently been included in the coordinated efforts of the Department of Energy and the Electric Power Research Institute (EPRI) in the reliable advanced liquid fuel engine preliminary design studies.[2]

Aerodynamic Design

The inherent benefits of low-aspect-ratio blading have been investigated by P&WA and others in recent years, beginning with single-stage rig test programs[3,4] and proceeding through full-scale multistage rig development programs. The test results have consistently demonstrated the capability of low-aspect-ratio blading to achieve increased efficiency and stability at high axial compressor loading levels. The low-aspect-ratio/high loading combination results in fewer required stages and fewer airfoils per stage for a given overall compressor pressure ratio. The larger geometry low-aspect-ratio blades can also provide improved durability and increased performance retention in extended operation.

Significant advances have also been made in the past decade in centrifugal compressor technology such that performance approaching that of axial compressors can be obtained especially in low-flow, low-pressure-ratio applications. This makes the centrifugal compressor stage attractive for use as a back end stage, where a single rugged certifugal stage can replace a number of small axial stages. The utilization of the centrifugal compressor stage thus can result in a further reduction in the number of required stages where frontal area is not a critical constraint (such as in stationary gas turbines). The combination of the centrifugal stage with low-aspect-ratio axial compressor aerodynamics in the current configuration allows the achievement of 18:1 pressure ratio on a single spool with high efficiency and 80% fewer parts as compared to current industrial gas turbine compressors.

The selection of the final compressor flowpath geometry (Fig. 2) was the result of a comprehensive parametric and optimization study.[1] The study results indicated that the peak compressor performance potential could be attained with a six-stage axial/single-stage centrifugal compressor configuration with a 6.67/2.7 pressure ratio split. An inlet airflow rate of 70 lbm/s was selected to be compatible with an advanced industrial gas turbine application in the 15,000 shp/10 MW class. Rotor speed was set at 15,000 rpm based on turbine stress limitation considerations.

Axial Compressor

The objective of the axial compressor aerodynamic design was to exploit to the maximum extent possible, without jeopardizing near-term applicability, the potential of low-aspect-ratio blading to achieve high aerodynamic loading levels with high efficiency and good stability. An aggressive

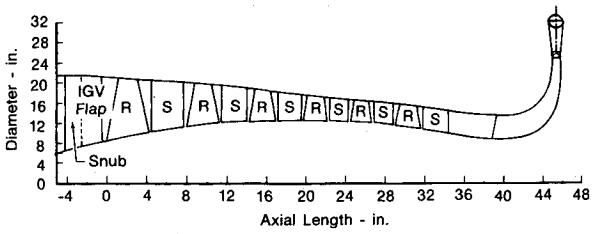

Fig. 2 Axial/centrifugal compressor flowpath.

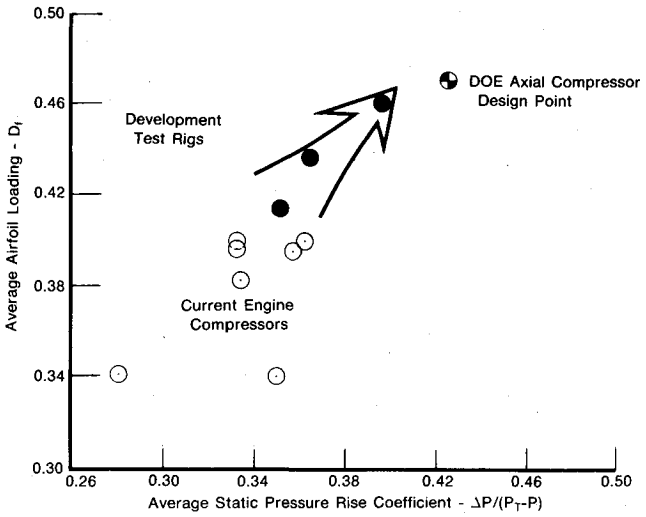

Fig. 3 Axial compressor loading comparison.

Table 1 Axial compressor airfoil series selection

Blade row	No. airfoils	Airfoil series[a]
IGV	13	63
R1	18	MCA
S1	20	CA
R2	21	MCA
S2	22	CA
R3	25	CA
S3	24	65/CA
R4	27	CA
S4	26	65/CA
R5	27	65/CA
S5	26	65/CA
R6	25	65/CA
S6	20	400

[a] MCA = multiple circular arc. CA = circular arc. 65/CA = 65 series thickness distribution superimposed on a circular arc meanline.

loading limit was therefore set (Fig. 3) which, although providing an approximate 15% increase in loading levels over current production engine compressors, represented a logical next step advancement in the state-of-the-art relative to previous multistage compressor development test rig programs. The 0.4 inlet hub/tip ratio, bulged i.d. flowpath evolved as the flowpath which provided the best efficiency/loading trade while maintaining a low-loss transition to the centrifugal stage.

The airfoil series selection for each of the axial compressor blade rows, along with the number of airfoils in each row, are given in Table 1. The selection of airfoil blading geometry for each blade row was made on the basis of optimizing airfoil performance for the particular Mach number regime for that row. Multiple circular arc airfoils were used for the first-stage rotor, which had an inlet tip relative Mach number of 1.20 at the design 1376 ft/s tip speed, and the second-stage rotor, which had an inlet tip relative Mach number of 1.05. Airfoil

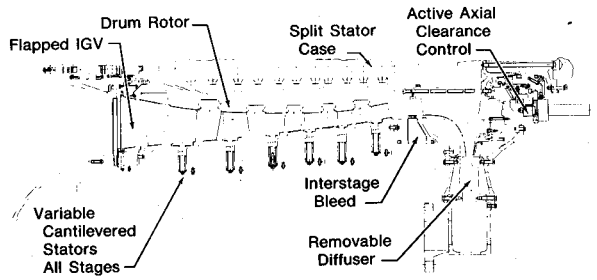

Fig. 4 Axial/centrifugal compressor rig cross section.

aspect ratios varied from 1.35 for the first rotor to 0.8 for the sixth-stage stator.

Centrifugal Stage

The centrifugal stage design incorporates a 25 deg backswept impeller and a 2:1 area ratio conical pipe diffuser designed to produce a stage pressure ratio of 2.7:1 (total-to-total). The design point inlet corrected speed and flow are 11,182 rpm and 14.1 lbm/s, respectively, which results in a specific speed of 64.

The centrifugal impeller has 18 full blades with one set of splitter blades. The inducer region of the impeller was modified slightly to accommodate the leading-edge geometry of a 400-series axial compressor airfoil and incidence was set to obtain minimum loss based on axial compressor cascade data. The axially defined leading-edge geometry was then smoothly transitioned into the conventional impeller blading. The mean impeller diffusion ratio (w_{max}/w_{min}) of 1.57 is within previously demonstrated P&WA design experience. Impeller discharge Mach number is 0.88.

The impeller discharge flow is further diffused to a Mach number of 0.83 in a short vaneless/semivaneless space region prior to entering the diffuser passages. Each of the 26 conical diffuser passages consists of a 3 deg cone angle segment to a 1.2:1 area ratio followed by a 5 deg cone angle segment to 2:1 area ratio (which results in a design exit Mach number of 0.35). A constant diameter throat length of 0.100 in. was included to reduce the sensitivity of the throat area to manufacturing deviations and leading-edge wear.

Test Rig

Based on the compressor aerodynamic design defined for the conceptual engine, a compressor test rig (Fig. 4) was configured for use in the component validation testing phase of the program. Where practical from time and budget standpoints, materials and fabrication techniques used for the major rig hardware items were selected to be compatible with those that would be used in an engine application. Design life goal was 20,000 h/10,000 cycles.

Rotor Assembly

The low-aspect-ratio axial compressor blades are mounted in a single-piece drum rotor. Blades for stages 2 through 6 are loaded circumferentially into annular grooves in the disk through loading slots provided on diametrically opposite sides of the rotor. Blade locks on the side of each loading slot secure the final blade inserted. The first-stage blade attachment is a conventional axial lug configuration in order to obtain sufficient lug shear area at the relatively small first-stage bore diameter. Rubber seals applied to the under side of the blade platforms are utilized to minimize leakage into the attachment cavities for all stages. An abrasive coating consisting of a mixture of 97% aluminum oxide and 3% titanium dioxide was applied to the drum rotor flowpath between blades to provide stator tip rub protection.

The centrifugal impeller is attached to the axial compressor drum rotor by means of a Curvic ® coupling and 12 tiebolts. A photograph of the complete rotor assembly is shown in Fig. 5.

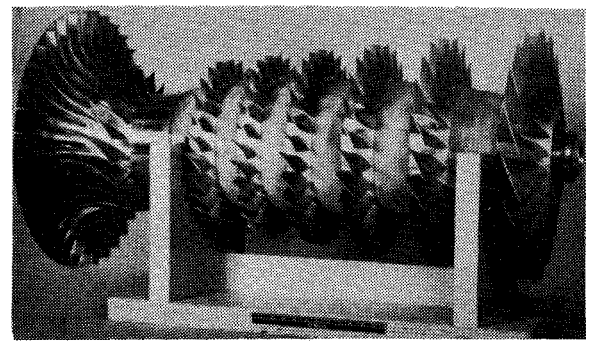

Fig. 5 Compressor rotor assembly.

Both the centrifugal impeller and axial compressor drum rotor were machined from solid Inconel 718 forgings. Titanium 6A1-4V was selected for the axial compressor rotor blades.

The rotor assembly is supported by a roller bearing on the front end, while a dual-bearing configuration is used in the rear in which a roller bearing carries all the radial load and a ball bearing carries all the thrust load. The ball bearing retainer can be moved axially to adjust the position of the compressor rotor relative to the cases and provide active control of the impeller-to-shroud tip clearance. All three bearings are under-race cooled with holes provided through the inner race to direct oil to the cage riding surfaces and rolling elements. Hydraulically damped bearing hairsprings are utilized for both roller bearings with spring rates selected to achieve a 20% rotor critical speed margin.

Stationary Cases

All of the front bearing compartment and slip ring services, including instrumentation routing, are provided through 13 inlet struts. Flapped inlet guide vanes are mounted immediately adjacent to each strut and are hydraulically driven through a sync ring to provide the desired rig inlet air angle.

The six stages of variable cantilevered stators are mounted in two horizontally split case halves. To minimize endwall leakage losses the leading edge of each stator, where the maximum pressure differentials occur, are entirely supported by the stator support button with the airfoil trailing edge cantilevered off the back of the button. A nominal 0.016 in. thick abradable coating of ekonol-aluminum was applied to the stator airfoil tips to work in conjunction with the drum rotor abrasive coating to provide rub protection. A silicone rubber rub strip material was included in the case o.d. flowpath wall over each rotor blade tip region for rotor rub protection.

The impeller shroud is bolted to its outer support case at the impeller exit with the inlet end of the shroud allowed free axial movement. Piston rings are used to seal the shroud inlet. The shroud has a 0.003-0.005 in. thick silver coating to minimize the effects of a minor rub should one occur. An interstage compressor bleed capability of up to 30% of the inlet flow rate is provided just forward of the impeller shroud for starting and off-design compressor matching.

The compressor rig hardware was designed to be compatible with two diffuser configurations: 1) a vaneless diffuser for use during the axial compressor documentation portion of the test program, and 2) a conical pipe diffuser for use during the overall compressor performance documentation testing. Capability was provided to change diffuser configurations on the test stand without dismounting the rig. Flow from the diffuser is discharged into an annular collector which has six exhaust flanges connected to the facility discharge ductwork.

Instrumentation

The compressor aerodynamic instrumentation was selected to accomplish three primary objectives: 1) define the overall

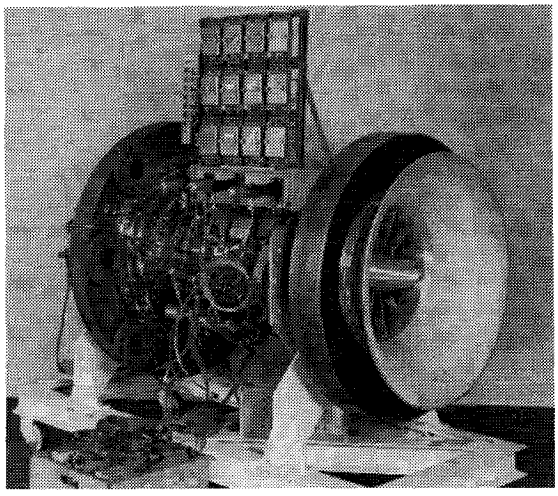

Fig. 6 Compressor test rig.

compressor performance, 2) allow definition of the axial compressor and centrifugal stage component performance, and 3) provide interstage measurements for diagnostic purposes to aid in performance optimization. Overall performance instrumentation consisted of measurements of total pressure and temperature at the compressor inlet (station 1.0) and discharge (station 3.0). Compressor inlet conditions were measured in the test facility inlet plenum chamber utilizing three Rosemount precision resistance temperature sensors and four standard total pressure sensors. Compressor exit conditions were measured at the centrifugal stage pipe diffuser exit plane. Four total pressure rakes and four total temperature rakes were utilized, each containing five individual Kiel-head sensors. Each rake was located at the exit of a different diffuser pipe with the probe sensors placed so that the superimposed array for each sensor type would cover 17 equal flow area segments with the center sensors on each rake providing redundant measurements of the center area.

Measurements of total pressure and temperature were also provided at the axial compressor discharge (station 2.0) just upstream of the interstage bleed to allow calculation of the axial and centrifugal compressor component performance. This instrumentation consisted of five circumferential wake rakes distributed radially across the flowpath. Each rake had eight pressure and eight temperature sensors alternated across the probe head to define the pressure and temperature gapwise distributions. The pressure sensors were impact tubes while the temperature sensors were Kiel-head stagnation tubes.

Structural instrumentation was provided primarily to monitor and evaluate the vibratory characteristics of the axial compressor airfoils. A total of 60 strain gages were utilized for this purpose, including 34 dynamic gages located on the blades and 26 dynamic gages located on the vanes.

A photograph of the fully assembled and instrumented compressor rig ready for shipment to the test stand is shown in Fig. 6.

Test Program

Test Facility

Demonstration testing of the axial/centrifugal compressor rig was conducted in the full-scale compressor test stand located in P&WA/GPD's Turbojet Engine Altitude Test Facility. The drive system for this facility consists of a single-stage, direct-drive TF30-P414A high-turbine module which has been adapted to run on high-pressure steam. The stand has the capability of providing 26,000 hp at 16,200 rpm over a wide range of pressurized and heated inlet conditions. Operation of the current program, however, required a throttled inlet (approximately 10 psia) due to the unavailability of one of the three facility boilers at the time the test program was being conducted.

The facility atmospheric inlet system includes a 132 ft long, 60 in. diam duct which is connected to a 14 ft long, 144 in. diam plenum chamber. The flow rate is measured by means of a standard ASME thin-plate orifice which is located in the 60 in. diam duct section. Both 15 and 24 in. diam orifices were used during the test program depending on the anticipated flow range of the particular test sequence scheduled.

The compressor test rig was installed in the facility by means of a free-standing mount aligned to the rotating centerline of the drive turbine. The compressor rotor was coupled to the drive turbine rotor utilizing a tight-fitting splined drive coupling. The compressor discharge air was ducted from the rig discharge collector through six 4 in. lines. Four of these lines were manifolded together into an 8 in. duct containing both an 8 in. main discharge control valve and a 2 in. vernier control valve, which were regulated as required during the test program to vary the compressor back pressure. The remaining two lines each contained a manually operated gate valve and a surge pop-bleed relief valve.

Run Program

The compressor test program was conducted in three phases. The initial phase of the compressor test program was structured to verify satisfactory operation of the compressor rig and all of its auxiliary support systems. During this test sequence, vibration and strain gage data were monitored and recorded continuously.

In the second test phase, axial compressor steady-state data were acquired along a series of speedlines from wide-open discharge to peak efficiency at 50, 70, 80, 90, 95, and 100% design speed. In order to obtain an early estimate of the axial compressor stability, additional data were obtained at 50 and 70% speed above the nominal operating line to approximately 20% stall margin.

The final phase of the test program was conducted to document the overall compressor performance over the complete operating range. For this phase, the vaneless diffuser, which had been installed for the prior two phases, was replaced with a pipe diffuser. The test sequence was specifically conducted to obtain the following data:

1) Starting and low speed aerodynamics.
2) Interstage bleed requirement definition.
3) Aerodynamic design point performance.
4) Axial, centrifugal, and overall compressor performance (pressure ratio, speed flow, and efficiency characteristics).
5) Surge line definition.

Performance Calculations

Overall compressor performance was defined from the compressor rig inlet plenum (station 1) to the pipe diffuser exit plane (station 3). The redundant low-velocity inlet measurements were arithmetically averaged, while the pipe diffuser exit temperature and pressure arrays were mass averaged to obtain representative mean values for use in the performance calculations. All calculations were performed on a total-to-total basis. Overall adiabatic efficiency was calculated based upon the overall pressure ratio and dry air values of enthalpy

$$\eta_{ad_{1,3}} = \frac{\Delta h'}{\Delta h} = \frac{f(PR_{1,3}T_1)}{f(T_1, T_3)} \tag{1}$$

A net adiabatic efficiency was also defined for the part-speed overall compressor performance which accounts for the work done on the interstage bleed flow. The net efficiency is defined as

$$(\eta_{ad})_{\text{net}} = \frac{(W - W_{bl})\Delta h'_{1,3}}{(W - W_{bl})\Delta h_{1,3} + W_{bl}\Delta h_{1,2}} \tag{2}$$

Polytropic efficiency was calculated from the adiabatic efficiency and pressure ratio assuming a γ of 1.4

$$\eta_p = \left[\frac{\gamma-1}{\gamma}\ell nPR\right] \Big/ \left[\ell n\left(1+\frac{PR^{(\gamma-1)/\gamma}-1}{\eta_{ad}}\right)\right] \quad (3)$$

A constant-flow stall margin definition was used as follows:

$$SM\% = \frac{PR_{surge} - PR_{op}}{PR_{op}} \times 100 \quad (4)$$

Performance for the axial and centrifugal stage components was determined in a manner similar to the overall performance except for using the total pressures and temperatures measured at the axial compressor discharge plane (station 2).

Uncertainty Estimates

Data acquired from the compressor rig were examined for consistency and validity and a detailed uncertainty analysis performed. The uncertainty analysis included an evaluation of potential sources of error due to the measurement sensors, the data acquisition and recording equipment, calibration data curve fits, data reduction procedures, sampling rates, and run-to-run measurement variations. The predicted uncertainties in the compressor rig inlet and discharge measurements used in the determination of the overall compressor performance are shown in Table 2. The resultant estimated uncertainty of the overall compressor efficiency is 1.31%.

Results

Overall Compressor Performance

An overall compressor performance map is presented in Fig. 7. The peak design speed overall performance measured was 87.8% adiabatic efficiency at 18.45:1 pressure ratio and approximately 10% stall margin. Performance for the data point closest to the 18:1 pressure ratio design point was 87.6% adiabatic efficiency and 14% stall margin. The demonstrated performance for these two points is compared to the contract goals in Table 3. Performance for the data point closest to the design pressure ratio exceeds the contract efficiency goal by 2.0% and exceeds the contract minimum stall margin goal by 4.0%. The highest efficiency measured at any speed (neglecting bleed effects) was 88.76% adiabatic efficiency at 12:1 pressure ratio and 90% rotor speed. All data were acquired with the variable axial compressor vane rows in their nominal positions per the design vane angle schedule. Part-speed interstage bleed flow rates were selected to insure adequate flow range capability at each of the speeds documented. No attempt was made to optimize or minimize the bleed flows. The approximate percent bleed at peak efficiency for each speed line is indicated in Fig. 7. Since the overall performance data were acquired at slightly reduced inlet pressure, the value of the test Reynolds number index ($\delta/\theta^{1.24}$) is also included on the figure for each speed line.

Part-speed efficiency values were also calculated with a correction to account for the work done on the interstage bleed flow. The resultant "net" overall performance map, which is useful for simplified cycle analyses which cannot separately book-keep the bleed flow, is presented in Fig. 8. It should be iterated that no attempt was made to minimize the part-speed bleed flow rates, hence improvement in the part-speed "net" performance relative to that shown is feasible.

Table 2 Uncertainty estimate

Variable	No. of sensors	Bias, ±	Precision, ±	Uncertainty, ±
Plenum P_t, psia	4	0.047	0.014	0.061
Plenum T, °F	3	0.37	0.47	0.84
Discharge P_t, psia	20	3.23	0.294	3.52
Discharge T, °F	20	7.60	0.82	8.42
Efficiency, %	–	1.13	0.18	1.31

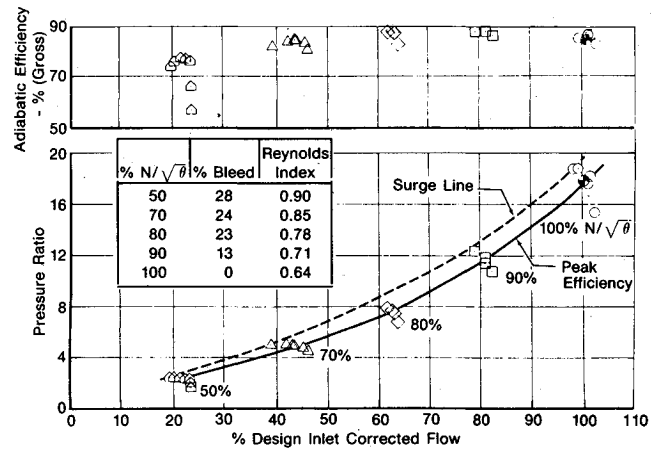

Fig. 7 Overall compressor performance map.

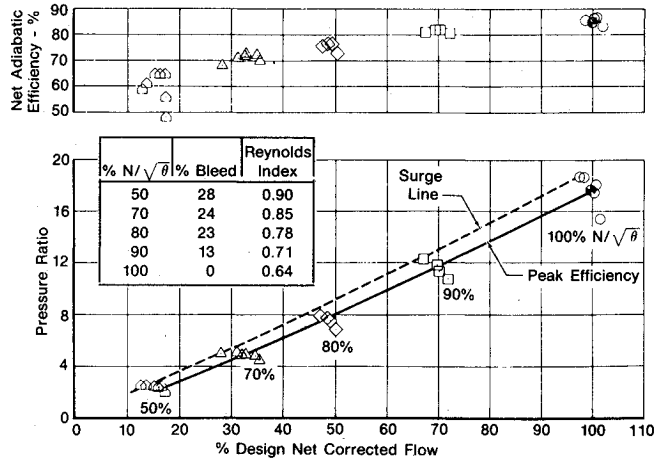

Fig. 8 Net overall compressor performance.

Table 3 Design speed overall performance summary

	Demonstrated		
	Peak efficiency	Closest to design pressure ratio	Program goal
Flow, lbm/s	70.7	70.5	70
Pressure ratio	18.45	17.81	18
Adiabatic efficiency, %	87.8	87.6	85.6
Polytropic efficiency, %	91.7	91.5	90
Stall margin, %	10.	14	10

Table 4 Centrifugal stage design speed performance summary

	Demonstrated		
	Peak efficiency	10% stall margin	Program goal
Pressure ratio	2.76	2.70	2.70
Airflow, lbm/s	14.19	15.20	14.10
Adiabatic efficiency, %	92.7	88.3	85.5
Exit Mach number	0.32	0.35	0.35
Stall margin, %	2.3	10.0	10.0

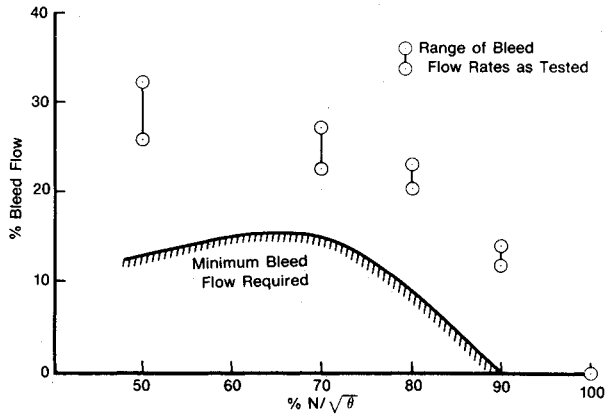

Fig. 9 Interstage bleed flow requirement.

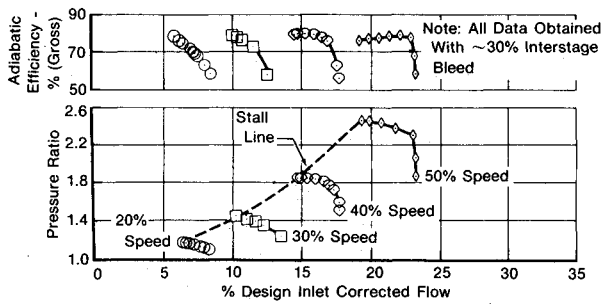

Fig. 10 Overall compressor low-speed performance map.

The pipe diffuser throat areas could also be rematched at a lower pressure ratio to further improve part-speed performance should that requirement exist for a particular application, but at the expense of a probable drop in design speed performance. An axial/centrifugal matching analysis was undertaken based on the available interstage data to determine the minimum bleed flow requirements at any given rotor speed with the design diffuser throat area. The results of the analysis are shown in Fig. 9, which summarizes the actual minimum bleed flows required as compared to the range of bleed flows utilized for the compressor test program.

Additional low-speed performance data were acquired from 20-50% design rotor speed (Fig. 10) to document the compressor starting characteristics. The compressor behavior in this region was surprisingly stable even during limited operation in the rotating stall region to the left of the "stall line" indicated on the figure. No compressor surges occurred at any time at these low speeds. Analysis of the low-speed data acquired indicated no starting problems which would complicate use of this compressor configuration in an engine application.

Axial Compressor Performance

Axial compressor performance data were acquired from both the vaneless and pipe diffuser portions of the test program. A composite performance map showing the axial

Table 5 Impeller/diffuser design point performance summary

	Demonstrated	Program goal
Impeller		
Pressure ratio	2.82	2.82
Adiabatic efficiency, %	94.7	90.0
Diffuser		
Total pressure loss, %	2.1	4.2

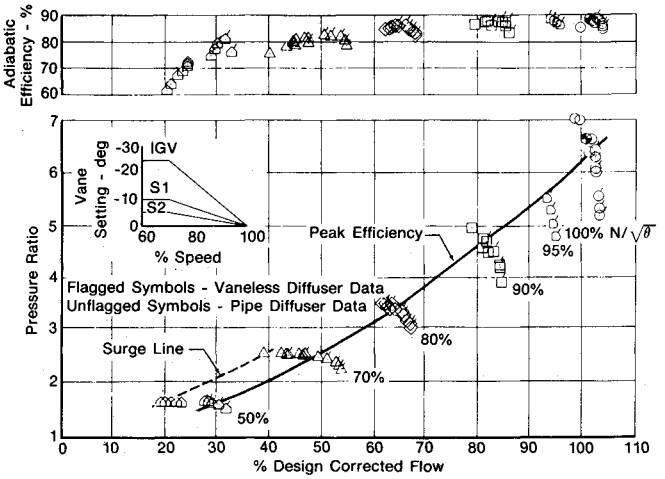

Fig. 11 Axial compressor performance map.

compressor performance data from both test sequences is shown in Fig. 11. The highest axial compressor performance was measured during the initial vaneless diffuser test sequence. Peak design rotor speed performance was 89.47% adiabatic efficiency at 6.5:1 pressure ratio (as compared to design goals of 89.0% adiabatic efficiency at 6.67:1 pressure ratio). The design rotor speed performance acquired at the same pressure ratio during the subsequent pipe diffuser testing was approximately 0.7% lower in efficiency. Cause of the performance deterioration can be primarily attributed to slightly increased "nominal" airfoil running tip clearances for the later test runs due to wearing away of the abradable rub materials during transient operating conditions.

A cursory analysis of the axial compressor stage characteristics indicates the compressor surges recorded at 50 and 70% rotor speeds were initiated in the axial compressor front end stages. The high-response instrumentation included in the test rig was not sufficient to distinguish in which component (the axial or centrifugal stages) the design speed surge initiated. Stall margin for the axial compressor at design speed from the axial compressor peak efficiency point to the overall compressor surge point was approximately 14%. The axial compressor stall margins at 50 and 70% rotor speeds were approximately 30 and 26%, respectively.

Centrifugal Stage Performance

All of the centrifugal stage performance goals were either met or exceeded as summarized in Table 4. An analysis of the

design rotor speed centrifugal stage performance at peak efficiency was conducted to divide the measured stage performance into impeller and diffuser component performances. Impeller exit conditions were calculated from the continuity and momentum equations based on the measured impeller exit static pressure and stage temperature rise. Design blockages were assumed. The resultant component performances are summarized in Table 5 relative to the design goals. The analysis indicates that the excellent stage performance demonstrated is the result of both higher than predicted impeller efficiency and lower diffuser total pressure loss.

Rig Mechanical Performance

The rotor dynamics of the compressor were excellent over the entire operating range. All of the observed rotor responses occurred at low speeds, were well within the allowable operating limits of the rig bearings, and could be accelerated/decelerated through without impact on the test rig operation.

The low-aspect-ratio blading vibratory stress levels observed during the compressor test program were also well below allowable limits. No rotor blade row vibratory stress level greater than 60% of the allowable was recorded at any time during the test program. Vibratory stress levels for the test vanes were an even smaller percentage of their allowables than those for the blades. In general, the vibratory data revealed good correlation between the predicted natural frequencies and the observed resonance conditions, particularly for first bending and first torsional mode response.

Conclusion

The compressor performance demonstrated not only exceeded the program goals, but even more significantly represents the highest known single-spool compressor performance demonstrated to date in this pressure ratio and flow class. This performance can be directly translated into equivalent benefits in terms of gas turbine engine performance potential. For the conceptual engine cycle defined (18:1 pressure ratio and 2500°F combustor exit temperature) each percent increase in compressor adiabatic efficiency can be equated to an approximate 1.0% improvement in simple cycle engine specific fuel consumption and an approximate 1.4% increase in shaft horsepower. The results are that much more significant when viewed in light of the fact that they were achieved at axial compressor aerodynamic loading levels 15% above current engine design practice.

The test results conclusively verify the readiness of the advanced low-aspect-ratio axial compressor and centrifugal backend stage technologies for incorporation in future industrial gas turbine applications. No mechanical, structural, or low-speed starting problems were encountered which would preclude use of the compressor configuration in an engine application. The technologies demonstrated are additionally potentially applicable to a wide range of advanced engine applications including small gas turbines, marine propulsion systems, and high-bypass-ratio turbofan engines.

Acknowledgment

The work presented in this paper was conducted for the U.S. Department of Energy, Office of Coal Utilization under Contract DE-AC05-760R05035.

References

[1] Schweitzer, J.K. and Brown, B.T., "Advanced Industrial Gas Turbine Technology Readiness Demonstration Program, Final Report, Phase I Design Study," U.S. Department of Energy, Washington, D.C., Rept. HCP/T 5035-0001, Oct. 1977.

[2] Boenig, F.H. and Day, D.L., "Compressor Configuration and Design Optimization for the High Reliability Gas Turbine," United Technologies Corp., Power Systems Division, South Windsor, Conn. Rept. GTR-2136, April 1980.

[3] Cheatham, J.G., et al., "Single-Stage Experimental Evaluation of Low Aspect Ratio, Highly Loaded Blading for Compressors, Part IX Final Report, Stage F and G, Volume I," NASA CR-134993, May 1976.

[4] Reid, L. and Moore, R., "Experimental Study of Low Aspect Ratio Compressor Blading," NASA TM 79280, March 1980.